RESEARCH PAPER

The Effect of Tin Concentration on Microstructural, Optical and Electrical Properties of ITO Nanoparticles Synthesized Using Green Method

Mala Siddaramappa[1], Haraluru Kamala Eshwaraiah Latha[1,*], Haraluru Shankaraiah Lalithamba[2], Andi Udayakumar[3]

***** *lathahke@gmail.com*

[1]Department of Electronics and Instrumentation Engineering, Siddaganga Institute of Technology, Tumakuru, India

[2]Department of Chemistry, Siddaganga Institute of Technology, Tumakuru, India

[3]Materials Science Division, Council of Scientific and Industrial Research-National Aerospace Laboratories, Bangalore, India

Received: June 2021 **Revised: August 2021** **Accepted: September 2021**

DOI: 10.22068/ijmse.2284

Abstract: *Indium tin oxide (ITO) nanoparticles were synthesized by green combustion method using indium (In) and tin (Sn) as precursors, and Carica papaya seed extract as novel fuel. This paper highlights the effect of tin concentration (5%, 10%, and 50%) on the microstructural, optical, and electrical properties of ITO nanoparticles (NPs). The indium nitrate and tin nitrate solution along with the fuel were heated at 600°C for 1 h in a muffle furnace and obtained powder was calcinated at 650°C for 3 h to produce ITO NPs. The above properties were investigated using XRD, FTIR, UV-Vis spectroscopy, SEM, TEM, and computer-controlled impedance analyzer. The XRD, SEM, and TEM investigations reveal the synthesized NPs were spherical in shape with an increase in average grain size (17.66 to 35 nm) as Sn concentration increases. FTIR investigations confirm the In-O bonding. The optical properties results revealed that the ITO NPs band gap decreased from 3.21 to 2.98 eV with an increase in Sn concentration. The ac conductivity of ITO NPs was found to increase with an increase in Sn concentration. These synthesized ITO NPs showed excellent properties for emerging sensor and optical device applications.*

Keywords: *Indium tin oxide, green synthesis, crystallite size, band gap, grain boundary, ac conductivity.*

1. INTRODUCTION

Sensors are used to measure the physical parameters (pressure, load, force, vibration) under the harsh environment such as high temperatures, high radiation, chemical corrosion in industrial applications. The sensitivity and accuracy of sensors depend on the sensing material and its composition. Silicon-based sensors are widely used in industrial applications. But these sensors cannot be used at high temperature applications because their electrical properties deteriorate above 150°C and mechanical properties above 500°C due to their narrow bandgap. Consequently, the material with good conductivity and wide bandgap is of interest for sensor applications at elevated temperatures [1-4]. Over the past few decades, researchers have focused on metal oxide-based sensors. Widely used metal oxides for sensor applications are indium tin oxide (ITO), zinc oxide (ZnO), cadmium oxide (CdO), titanium dioxide (TiO_2), and antimony tin oxide (ATO). Among these, Indium tin oxide (ITO) is a highly degenerative n-type semiconductor with low resistivity ($7x10^{-5}$ Ωcm), wide bandgap (3.2 - 4.3 eV), and exhibits good piezoresistive properties [5-7]. It has high optical transmittance in the visible region and excellent adhesion to substrates [8, 9]. In the optoelectronic industry it is widely used in liquid crystal screens, organic light-emitting diodes (OLEDs), and touch screens [10, 11]. Therefore, it is necessary to synthesize conductive and wide bandgap ITO material for sensor and optical device application.

ITO NPs can be synthesized using various synthesis methods such as physical method and chemical method. The physical method is time and energy-consuming, and deposition takes place at high temperature and pressure. The chemical method is simple, inexpensive, and low temperature synthesis. Various chemical methods such as sol-gel [12], hydrothermal [13, 14], coprecipitation [15, 16], method [17], and combustion are used for the synthesis of ITO NPs. Among these, the combustion method is more advantageous than other methods. By combustion method, it is possible to produce monophasic nano powders with homogeneous microstructure, at lower temperature or shorter reaction time [18-21]. Precursors and fuel are used in the combustion method for the synthesis of NPs. But

the use of toxic reducing (fuel) and stabilizing agents makes it harmful. Recently, green combustion synthesis has attracted researchers because it eliminates the use of toxic chemicals, consumes less energy, and produces safer products and by-products. It is easy, efficient, and eco-friendly method. Green combustion synthesis uses plant (flower, seeds, fruits, leaves, barks, roots) extract as fuel [22, 23].

For combustion reaction to occur effectively, the carbohydrate content of the fuel plays a major role. From the literature survey, it is evident that Carica Papaya seeds have good carbohydrate content, oil content, and fuel properties. Therefore, these seeds extract is used as fuel for the synthesis of NPs in the combustion method. Carica papaya belongs to the family of Caricaceae [24, 25]. This Carica papaya plant is majorly grown in India, Mexico, Florida, Australia, Srilanka, and South Africa. This paper presents a study that validates the strategy of green synthesis of ITO NPs using the green combustion method, with papaya seed extract as fuel and, In and Sn as precursors. The effect of Sn concentration on the microstructural, optical and electrical properties of ITO NPs are studied.

2. EXPERIMENTAL PROCEDURES

2.1. Materials

For the green synthesis of ITO NPs, In and Sn were used as precursors, Carica papaya seed extract as fuel, and distilled water as synthesis medium. The quality of raw materials used for synthesizing ITO NPs is tabulated in Table 1.

2.2. Preparation of Seed extract

The collected Carica papaya seeds were washed with de-ionized water and were sun-dried for 5 days.

The dried seeds were ground using a mixer grinder to obtain a powder of 15 g. Dried and powdered Carica papaya seeds were mixed with 50 mL of distilled water to prepare an aqueous solution. The obtained solution was heated by constant stirring for 1 h at 80°C, cooled, and filtered through Whatman No.1 filter paper (pore size 42 μm) to obtain seed extract. The obtained seed extract was used as a fuel for the synthesis of ITO NPs.

2.3. Mode of Synthesis

In ingots of 10 g were dissolved in 50 mL of nitric acid (HNO_3). Later 50 mL of distilled water was added slowly by constant stirring and was refluxed for 3 h. The obtained indium nitrate solution was placed in a magnetic stirrer for 18 h. 1.2 g of Sn was dissolved in 5 mL of HNO_3, 45 mL of distilled water, and stirred in a magnetic stirrer for 21 h to obtain tin nitrate solution. Indium nitrate solution of 5 mL, tin nitrate solution of 5 mL, and 15 mL of papaya seed extract were transferred to silica crucible and kept in a muffle furnace at 600°C for 1 h. The ITO layer formed on the sides of the silica crucible was scratched using a spatula and the nanopowder was calcinated at 650°C for 3 h to produce ITO of 5:5 composition. The same procedure was repeated for 9:1 and 9.5:0.5 composition of ITO NPs by keeping fuel extract constant (15 mL).

Process chart of green synthesis of ITO nano particles by combustion method is shown in Fig.1.

2.4. Characterization of ITO NPs

The green synthesized ITO NPs were characterized using various characterization techniques.

The crystal orientation of the ITO NPs was examined by X-ray diffraction (XRD) (Model: Rigako, smart lab, Japan, Monochromatized CuKα radiation with Ni filter) operated at 40 kV, 20 mA with CuKα (λ=1.542 Å) radiation as an X-ray source configured in symmetrical θ-2θ mode.

Table 1. Raw materials used for synthesizing ITO NPs.

Raw materials	Formulation	Purification (%)	Physical state	Manufacturer
Indium	In	99.99	Solid	Spectrochem
Tin	Sn	99.995	Solid	Qualigens fine chemicals
Nitric acid	HNO_3	71	Liquid	Fisher scientific

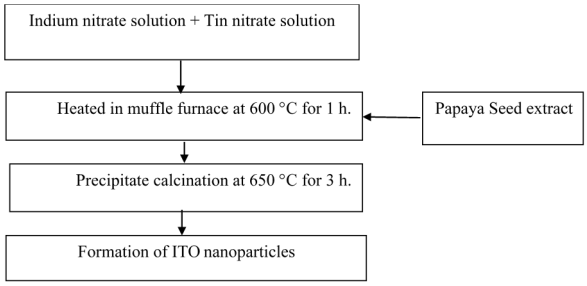

Fig. 1. Process chart of green synthesis of ITO NPs

FTIR analysis was carried out using Brucker Alpha-T spectrometer over the wavenumber of 400 to 4000 cm^{-1} with a spectral resolution of 4 cm^{-1}. UV-Vis spectroscopy (Model UV-3092) with wavelength numbers from 200 to 900 nm was used for optical studies. Pure barium sulfate powder ($BaSO_4$) was used as a standard for background measurement.

The finely ground ITO NPs were packed into the sample holder and then measured using a UV-Vis spectroscopy equipped with an integrated sphere accessory.

The morphology of ITO NPs was studied by scanning electron microscope (SEM with EDS) Carl Zeiss AG - ULTRA 55 and high-resolution transmission electron microscope (JEOL/JEM2100).

The conductivity and dielectric properties of synthesized ITO NPs were measured using a computer-controlled impedance analyzer (Model-IM 3536) at room temperature (RT) in the frequency range from 10 Hz to 8 MHz. To measure conductivity and dielectric parameters, ITO NPs were made into circular pellets of thickness 1.2 mm and diameter 1 cm using a hydraulic press (Model M-15) by applying pressure of 5 Tons. These pellets were placed between the electrodes of the impedance analyzer and measurements were carried out by applying 1V bias voltage.

3. RESULTS AND DISCUSSIONS

3.1. Microstructural Analysis

The XRD patterns of ITO NPs are shown in Fig. 2. The diffracted peaks indexed at 21.31°(211), 30.4°(222), 35.3°(400), 37.6°(411), 41.7°(322), 45.57°(431), 50.8°(440), and 60.5°(622) correspond to cubic bixbyite (JCPDS 06-0416) structure of ITO NPs. A strong peak was observed in all the samples at 2θ = 30.4° and corresponds to ITO (222) phase. The intensity of the peak (222) increases as the Sn concentration increases [26, 27] and the average lattice parameter was calculated and found to be 10.16 Å which is in good agreement with the literature [27-29].

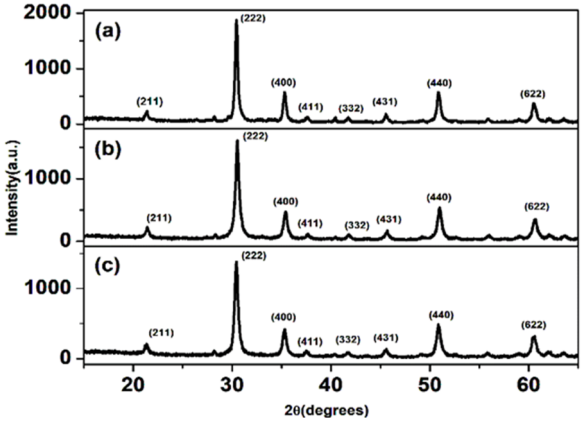

Fig. 2. XRD patterns of ITO NPs with (a) ITO 5:5 (b) ITO 9:1 (c) ITO 9.5:0.5

For the determination of the crystallite size and lattice strain contribution to the peak broadening, a graph was plotted between βcosθ and 4sinθ is shown in Fig. 3. A straight line was obtained with a slope equal to the strain and intercept equal to crystallite size [30]. The crystallite size (D) and lattice strain (Ɛ) of 4 high-intensity XRD peaks (222, 400, 440, and 622) were estimated from the W-H plot (Fig. 3).

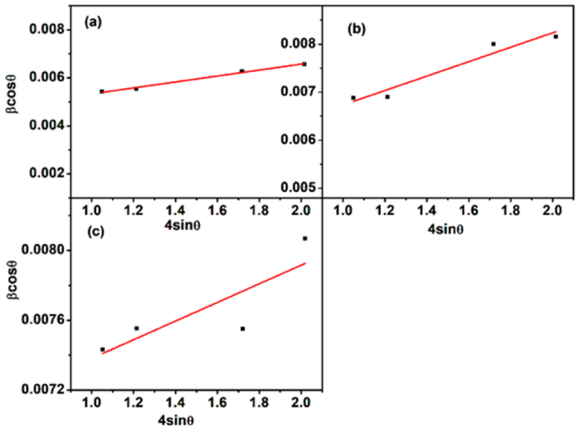

Fig. 3. W-H plots of ITO NPs with (a) ITO 5:5 (b) ITO 9:1 (c) ITO 9.5:0.5

It was observed that the Full width at half maximum (FWHM, β) decreases with an increase in Sn concentration (Table 2), which indicates an increase in crystallite size.

Table 2. Average crystallite size and lattice strain of ITO NPs

Sample	Peak Position 2θ(degrees)	(hkl)	FWHM (10^{-3} rad)	Average crystallite size D(nm)	Average lattice strain ϵ (10^{-4})	Lattice parameter (Å)
ITO 5:5	30.42	(222)	5.6	35.39	1.24	10.18
	35.31	(400)	5.8			10.16
	50.89	(440)	6.9			10.13
	60.54	(622)	7.6			10.13
ITO 9:1	30.43	(222)	7.1	27.62	1.91	10.17
	35.39	(400)	7.2			10.12
	50.98	(440)	8.8			10.12
	60.62	(622)	9.4			10.12
ITO 9.5:0.5	30.52	(222)	7.82	21.22	5.33	10.14
	35.40	(400)	7.8			10.16
	50.88	(440)	8.3			10.13
	60.52	(622)	9.3			10.13

This shows that Sn concentration is an important parameter that influences the crystallinity of ITO NPs [28, 29].

Lattice strain decreases as the Sn concentration increases because of an increase in grain size. The absence of SnO_2 peaks (Fig. 2) indicates the complete doping of Sn^{4+} ions into the In_2O_3 lattice.

Oxygen vacancies usually occupy the (400) plane and are not well occupied in the (222) plane. It was also observed from XRD spectra the intensity of the (400) plane increases as Sn concentration increases resulting in higher oxygen vacancies.

The intensity ratio of $I_{(400)}$ /$I_{(222)}$ plane for different Sn concentration is 30.86%, 30.48% and 29.85% for ITO 5:5, ITO 9:1 and ITO 9.5:0.5, respectively [27, 31, 32]. As Sn^{4+} concentration increases the ITO nanoparticles will be oriented towards the (222) plane and the I_{222} peak shifts towards lesser 2θ values [27, 32] as shown in Fig. 4.

The interchain separation length (R) for synthesized ITO NPs was calculated using the equation (1) for (222) peak. The R values for ITO NPs are 0.202 nm, 0.2045 nm, and 0.2238 nm for ITO 5:5, ITO 9:1, and ITO 9.5:0.5, respectively.

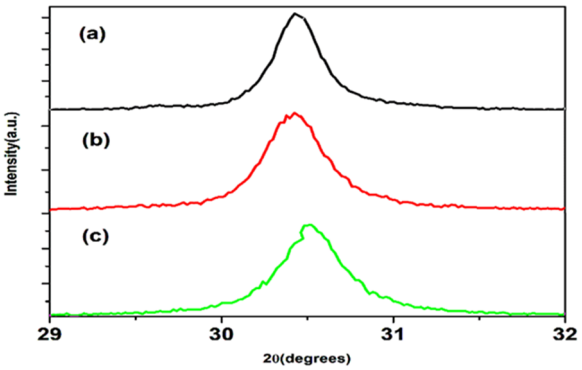

Fig. 4. Shift in I222 peak for different ITO NPs with (a) ITO 5:5 (b) ITO 9:1 (c) ITO 9.5:0.5

The NPs which have the shortest R-value will have the highest conductivity because when interchain separation length decreases, hopping of charge carriers increases.

$$R = \frac{5\lambda}{8sin\theta} \quad (1)$$

Where λ is the wavelength of the X-ray (Cu Kα) with value1.542 Å, 2θ is the location of diffraction peaks.

Fourier transform infrared spectra of papaya seed extract (Fig. 5) showed the presence of an aromatic C=C group at wavenumber 1448 and 1518 cm^{-1}.

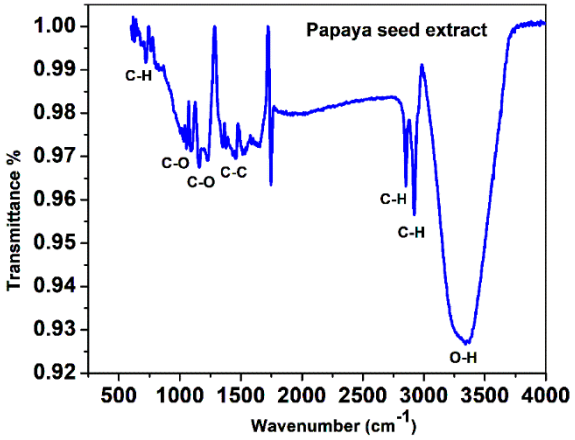

Fig. 5. FTIR spectra of papaya seed extract

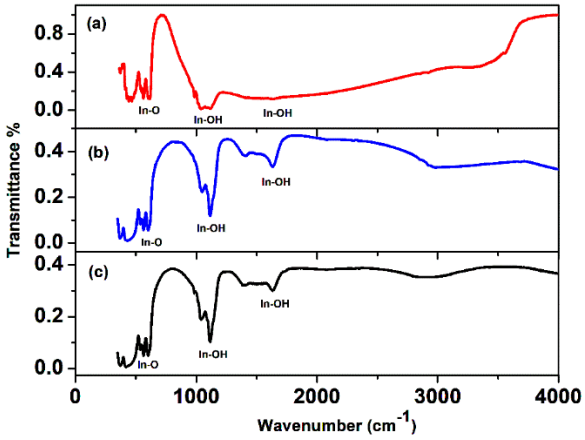

Fig. 6. FTIR spectra of synthesized ITO NPs with (a) ITO 5:5 (b) ITO 9:1 (c) ITO 9.5:0.5

The absorption peaks at 1100, 1157, and 1233 cm^{-1} were due to the C-O stretching vibration [33]. The peaks at 2846 and 2923 cm^{-1} show C-H stretching vibration, and the absorption peak at wavenumber 3341 cm^{-1} is due to the presence of -OH in Carica papaya seed extract. The transmittance peaks in the Fourier transform infrared spectra of ITO NPs are shown in Fig. 6. FTIR spectra exhibit the stretching vibrational peaks around 500 cm^{-1} to 600 cm^{-1} for synthesized ITO NPs with different Sn concentrations. Since the In-O bond is highly IR active, a vibrational peak appears at around 540, 560, and 600 cm^{-1} in ITO NPs [13, 17, 34].

The FWHM of the In-O bond peak was found to decrease with an increase in Sn concentration indicative of the increase in crystallinity and this result is in good agreement with the XRD result. The presence of OH in the precursor is found in the spectrum at two vibration modes 1000 to 1250 cm^{-1} and 1640 cm^{-1}, respectively. The vibrational peak intensity at around 1150 cm^{-1} was found to be decreased for ITO 9:1 and ITO 9.5:0.5 indicative of the transformation of hydroxyl precursor to oxide precursor. There are no vibrational peaks observed for Sn-O or Sn-O-Sn bonds.
Fig. 7 exhibits the SEM and TEM micrographs of green synthesized ITO NPs.

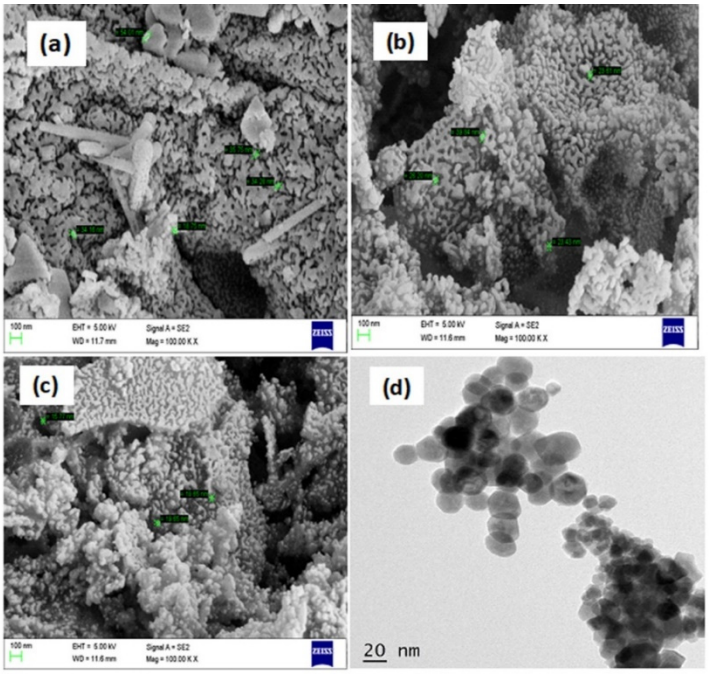

Fig. 7. SEM and TEM micrographs and EDS spectra of ITO nano particles (a) ITO 5:5 (b) ITO 9:1 (c) ITO 9.5:0.5 (d) TEM of ITO 9:1

The average grain size of synthesized ITO NPs was found to be 35 nm, 28.27 nm, and 17.66 nm for ITO 5:5, ITO 9:1, and ITO 9.5:0.5, respectively. This reveals that the grain size increases as the Sn concentration increases and the result is in good agreement with the XRD.

The ITO NPs with less Sn content exhibits spongy and more porous structures. As the Sn concentration increases fluffiness decreases. The less doped ITO NPs appear less dense, with more pores and cavities [17, 26, 27]. Therefore, more charge carriers are trapped in pores and cavities, which affects the conductivity of ITO NPs. TEM morphological analysis of ITO (9:1) NPs shows the spherical structure and is shown in Fig. 7d.

The elemental composition of synthesized ITO NPs is shown in Fig. 8. EDAX reports the presence of only In, Sn, and O, and no other impurities were observed. For high temperature sensor applications, it is necessary to know the bandgap of the ITO NPs. Hence the diffused reflectance spectrum of synthesized ITO NPs for different Sn concentrations were recorded at RT and is shown in Fig. 9.

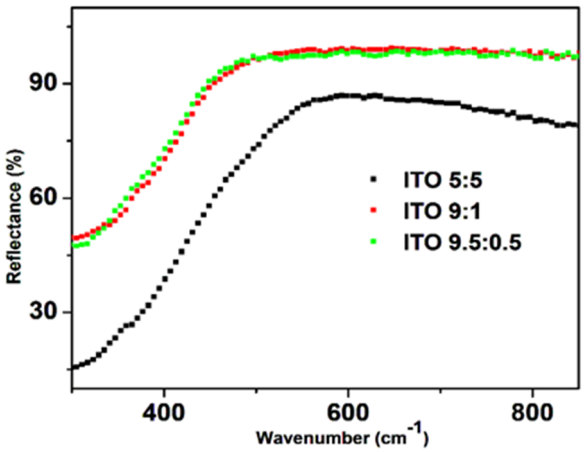

Fig. 8. Reflectance spectrum of ITO NPs.

The band gap of ITO NPs was determined by diffuse reflectance spectroscopy [17, 28, 29] using Kubelka-Munk function (F(R)) (2)

$$F(R) = \frac{(1-R)^2}{2R} \quad (2)$$

Where R is reflectance. The energy of photon E is calculated from (3)

$$E = \frac{hc}{\lambda} = h\nu \quad (3)$$

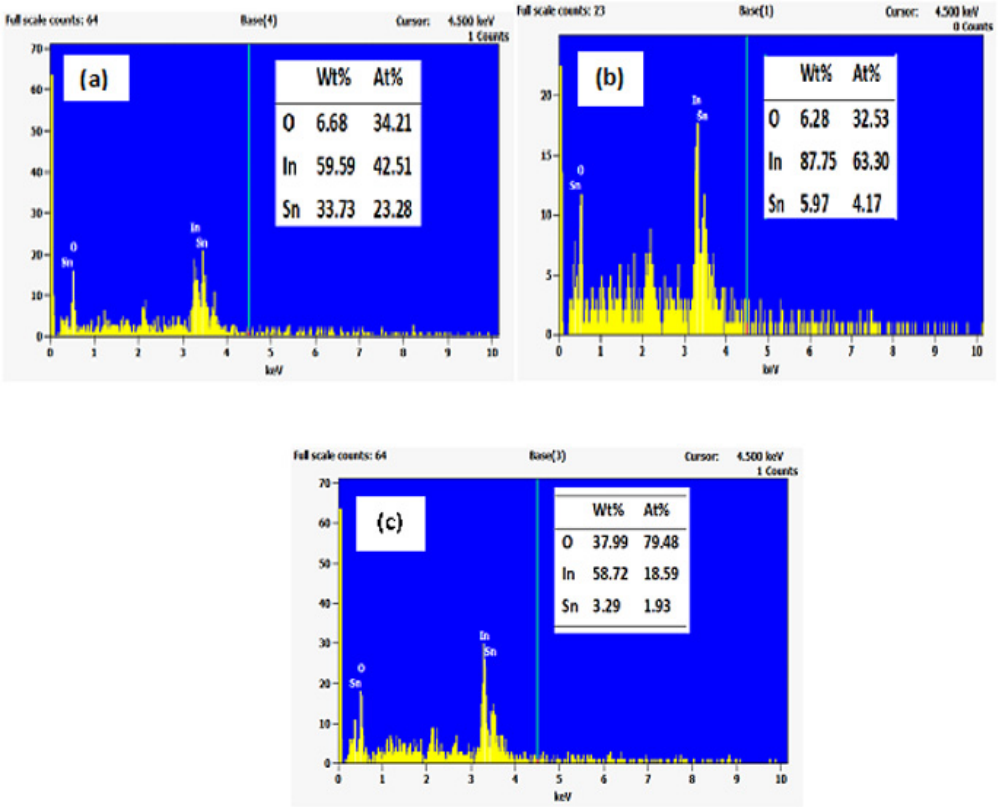

Fig. 9. EDAX spectra of ITO NPs (a) ITO 5:5 (b) ITO 9:1 (c) ITO 9.5:0.5

Where h is Planck constant ($6.63x10^{-34}$ Js), C is the speed of light in vacuum ($3x10^8$ m/s), λ is the wavelength of photon and ν is the frequency (Hz), respectively. Bandgap plots were obtained using Kubelka-Munk function and photon energy and are shown in Fig. 10.

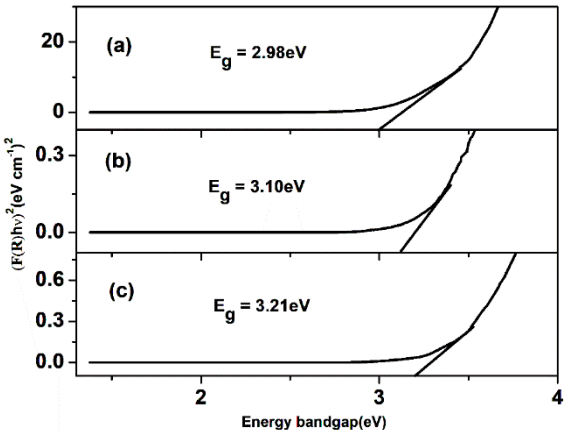

Fig. 10. Bandgap of ITO NPs with (a) ITO 5:5 (b) ITO 9:1 (c) ITO 9.5:0.5

The measured band gap was in the range of 2.98 to 3.21 eV for synthesized ITO NPs. A larger bandgap was obtained for small values of I_{400}/I_{222} ratio [32]. As Sn concentration increases, the bandgap decreases due to an increase in grain size and a decrease in the grain boundary. This requires less excitation energy for electrons to jump from one grain to another. As Sn concentration decreases, fewer oxygen vacancies are created in the ITO NPs that leads to a decrease in carrier concentration. Due to this bandgap is shifted to a higher value because of partially filling of conduction band by carriers.

3.2. Electrical parameter Analysis

It is essential to have knowledge of the conductivity of ITO NPs for sensor application. Hence conductivity and impedance plots were analyzed at RT for the synthesized ITO NPs. Generally, the effect of grain and grain boundaries for a wide range of frequencies can be explained with respect to the electrical properties of the material samples. The electrical properties of the material are normally explained in terms of dielectric constant (Ɛ*), complex impedance (Z*), and loss tangent (tan ∂). These are related to each other as $Ɛ^* = Ɛ^1 - j\,Ɛ^{11}$, $Z^* = Z^1 - jZ^{11}$ and $\tan ∂ = (Ɛ^{11}/Ɛ^1)$ where ($Ɛ^1$, Z^1) and ($Ɛ^{11}$, Z^{11}) are real and imaginary components [35-39].

The dielectric behavior of all synthesized ITO NPs was studied at RT by varying frequencies from 10 Hz to 8 MHz. The dielectric constant for different Sn concentration ITO NPs is shown in Fig. 11. The capacitance values obtained during the impedance analysis of ITO NPs were used to calculate the dielectric constant of ITO NPs using (4).

$$Ɛ^1 = \frac{C_p d}{Ɛ_0 A} \quad (4)$$

Where $Ɛ_0$ is the permittivity of free space, d is the thickness of the ITO pellet, A is the cross-sectional area of a flat surface of the ITO pellet and Cp is the capacitance of specimen in Farad (F).

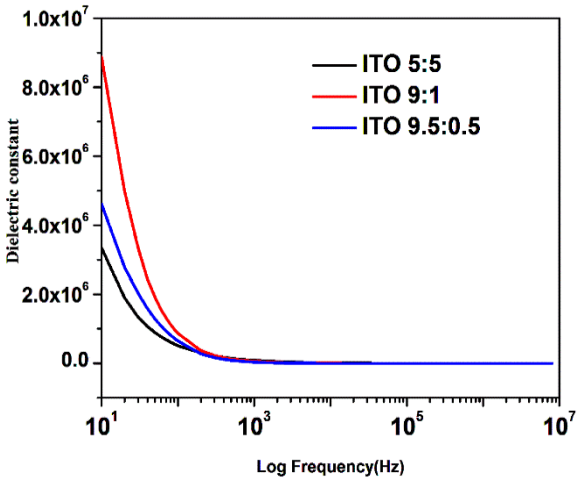

Fig. 11. Variation of dielectric constant ($Ɛ^1$) with respect to frequency of ITO NPs.

Result reveals that at lower frequencies the dielectric constant has got maximum value and was found decreasing as frequency increases (less than 1000 Hz) for all the synthesized ITO NPs and, becomes constant at high frequency (above 1000 Hz). This behavior can be explained using the Maxwell-Wagner interfacial model [35]. According to this model, the dielectric medium is considered to be composed of double layers, conductive grains, and resistive grain boundaries. Upon the application of electric field, charge carriers can easily migrate from grains but are accumulated at grain boundaries. This process can produce large polarization and dielectric constant. As frequency increases, the dielectric constant decreases because of the tendency of dipoles to orient themselves to the applied electric field. In the high-frequency region (above 1000 Hz), the dipoles will be hardly oriented to an applied field. Hence dielectric constant for ITO

NPs remains constant at the high-frequency region [35, 37].

Loss tangent (tan δ) represents the energy dissipation in the dielectric system. The variation of tan δ with frequency for ITO NPs at RT is shown in Fig. 12. The results reveal that, for samples, ITO 9:1 and ITO 9.5:0.5 tan δ will reach to its highest value because grain boundaries actively contribute at low frequency. Hence more energy for electron hopping is needed at low frequency. The peaking behavior occurs when the hopping frequency of electrons is equal to the frequency of the applied electric field. At the high-frequency region (above 10,000 Hz) tan δ decreases for all the compositions, which may be due to space charge polarization and hence conductivity increases for all the ITO NPs.

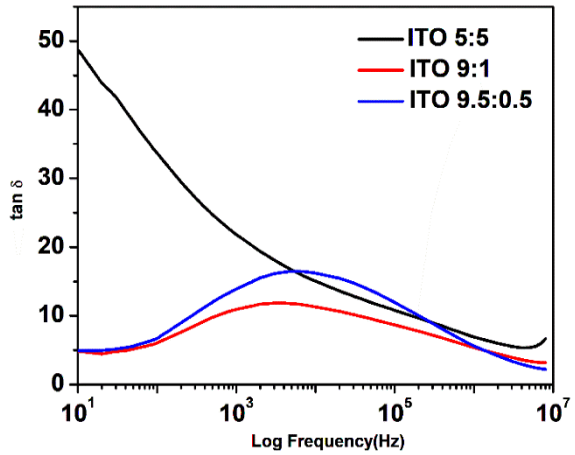

Fig. 12. Variation of loss tangent (tan δ) of ITO NPs with respect to frequency

The variation of ac conductivity with respect to change in frequency for different Sn concentrations of ITO nanoparticles measured at RT is shown in Fig. 13. The result reveals that ac conductivity increases with an increase in the frequency of applied ac field due to an increase in the electron hopping frequency. ITO 5:5 has high conductivity than the other two samples because, as the Sn concentration increases grain size increases, grain boundary decreases, and dielectric constant decreases, hence conductivity increases. This result is in good agreement with XRD (interchain separation length). Conductivity increases due to the release of the electron by substituting donor Sn^{4+} ion for In^{3+} ion in In_2O_3 as Sn concentration increases, which results in the generation of an extra electron into the conduction band and carrier density increases. Hence ITO 5:5 has more conductivity compared to sample ITO 9:1 and ITO 9.5:0.5 (Fig. 13).

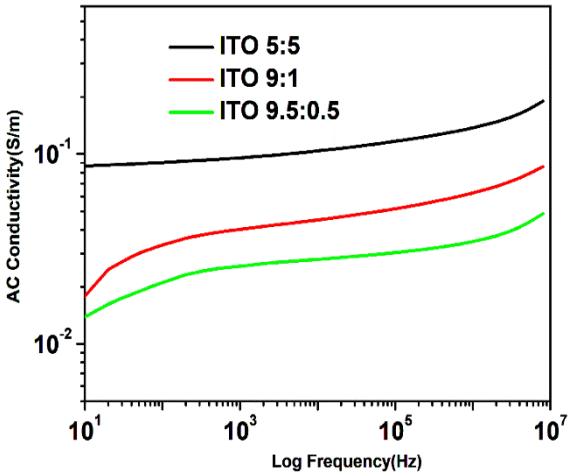

Fig. 13. Variation of ac conductivity of ITO NPs with respect to frequency.

The complex impedance spectrum of ITO samples shows the grain and grain boundary effect. Impedance data were present in the form of Z^{11}(capacitive) and Z^{1}(resistive). The impedance data were fitted into Zview software to obtain the Nyquist plots and electrical circuits with fitting parameters. Figs. 14 (a-c) show the complex impedance plot (as Nyquist plot) i.e., Z^{1} and Z^{11} over a wide range of frequencies from 10 Hz to 8 M Hz, and its equivalent circuit parameters are tabulated in Table 3. It was observed that the radii of semicircle vary as the Sn concentration varies. Generally, semicircle at higher and lower frequencies represents grain and grain boundary properties. For these ITO samples two semicircles were observed in the Nyquist plot, the first semicircle at high frequency represents the grain resistance (R_g) and the second semicircle at low frequency represents the resistance of grain boundary (R_{gb}).

The grain resistance and grain boundary resistance were measured for different ITO compositions and are tabulated in Table 4. The result shows that grain boundary resistance decreases as Sn concentration increases, which helps in the improvement of electrical conductivity.

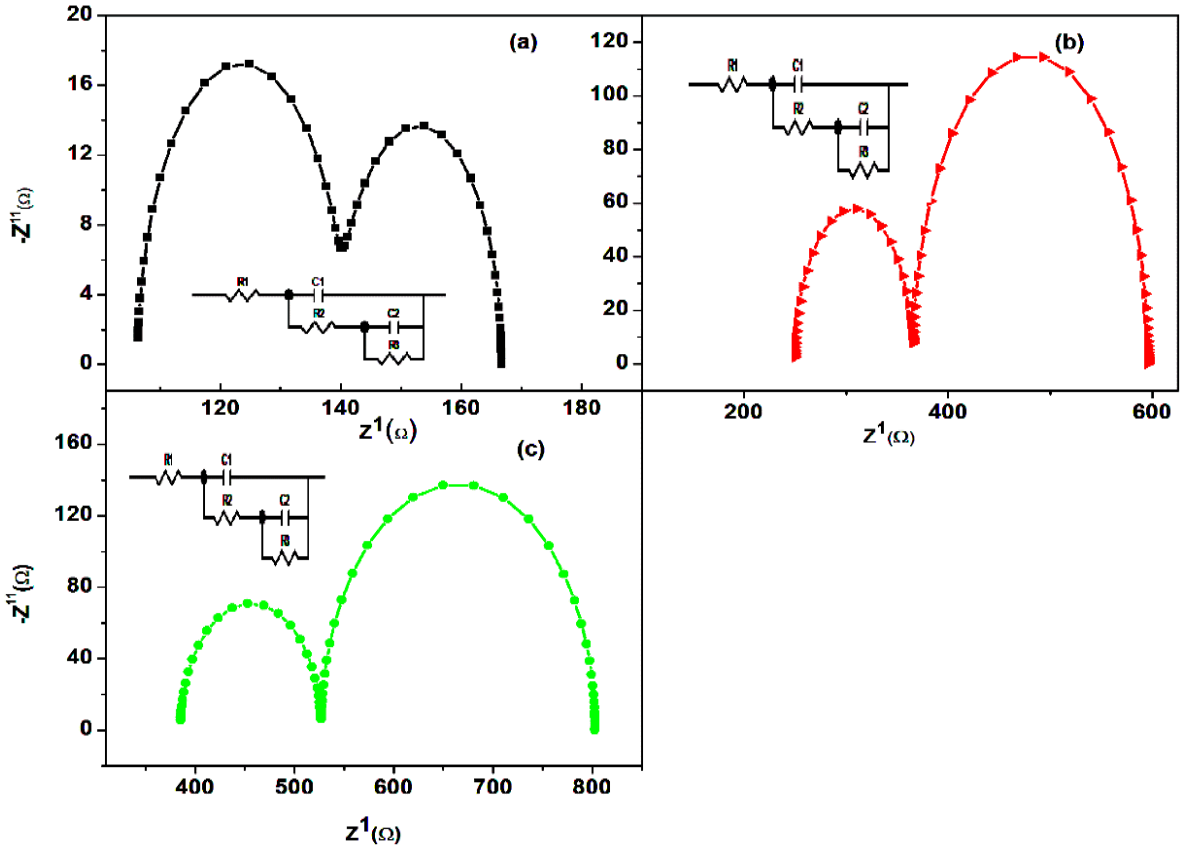

Fig. 14. Nyquist plots of ITO NPs and its electrical equivalent circuits inset. (a) ITO 5:5 (b) ITO 9:1 (c) ITO 9.5:0.5

Table 3. Equivalent circuit parameters obtained through impedance analysis.

ITO Composition	Equivalent circuit Parameter values				
	R1(Ω)	C1(F)	R2(Ω)	C2(F)	R3(Ω)
ITO 5:5	106.3	1.286E-8	34.51	1.36E-6	25.88
ITO 9:1	249.9	7.94E-9	115.9	6.93E-6	230
ITO 9.5:0.5	385.1	3.56E-9	141.9	7.21E-6	275.7

Table 4. Grain resistance and grain boundary resistance of ITO NPs.

Composition	Grain Resistance R_g(ohms)	Grain boundary Resistance R_{gb}(ohms)
ITO 5:5	34.51	25.88
ITO 9:1	115.9	230
ITO 9.5:0.5	141.9	275.7

The dc conductivity of ITO NPs (pellets) was studied by the 2 probe method by using Keithley 6221 current source and Keithley 2182A nano voltmeter.

The I-V characteristics obtained for different compositions of ITO NPs are shown in Fig. 15. The resistance values were obtained from the slope of I-V characteristics and dc conductivity was calculated from resistance, thickness, and area of pellets of ITO NPs for a different composition.

The dc conductivity values were found to be $1.04x10^{-3}$ S/m, $1.94x10^{-5}$ S/m, and $1.03x10^{-5}$ S/m for ITO 5:5, ITO 9:1, and ITO 9.5:0.5, respectively. The dc conductivity of ITO 5:5 is higher than the other two ITO compositions due to higher crystallite size, lower bandgap, and lower value of interchain separation length(R).

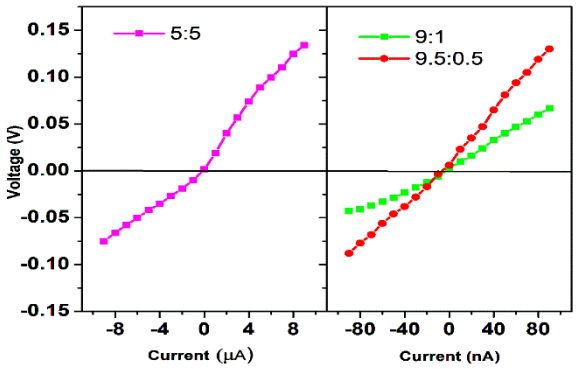

Fig. 15. I-V characteristics of ITO NPs of different compositions.

4. CONCLUSIONS

ITO NPs were successfully synthesized by the green combustion method using In and Sn as the precursor and Carica papaya seed extract as a novel fuel. The effect of Sn concentration on microstructural, optical and electrical properties of ITO NPs was analyzed. The XRD results reveal that the synthesized ITO NPs exhibits a cubic bixbyite structure with high crystallinity. Microstructural analysis reveals spherical structure with increasing grain size (17.66 to 35 nm) as Sn concentration increases. FTIR results confirm the presence of the In-O bond in synthesized ITO NPs. By increase in Sn concentration, the bandgap of ITO NPs is decreased (3.21 to 2.98 eV) which in turn affects the ac conductivity and dc conductivity of ITO NPs. AC conductivity and dc conductivity of ITO NPs increase as Sn concentration increases. Complex impedance plot exhibits both grain and grain boundary effect. Both grain resistance and grain boundary resistance decrease with an increase in Sn concentration. With an improved bandgap and conductivity, the ITO NPs with composition 9.5:0.5 are suitable material for the development of sensors and optical device applications.

5. ACKNOWLEDGMENTS

The authors thank Director and Principal of Siddaganga Institute of Technology, Tumakuru, Karnataka for the research facilities. One of the authors (H.K.E. Latha) is thankful to the vision group of science and Technology (VGST), Govt. of Karnataka for providing funds under CISEE programme (GRD No. 645) for carrying out the research work.

6. REFERENCES

[1] Shor, J.S., Goldstein, D., and Kurtz, A.D., “Characterization of n-Type β-SiC as a Piezoresistor”, IEEE Trans. Electron Devices, 1993, 40, 1093–1099.

[2] Okojie, R.S., Ned, A.A, Kurtz, A.D., Carr, W.N., “Characterization of highly doped n- and p-type 6H-SiC piezoresistors”, IEEE Trans. Electron Devices, 1998, 45, 785–790.

[3] Rasia, L. A., Mansano, R. D., Damiani, L. R., and Viana, C. E., “Piezoresistive response of ITO films deposited at room temperature by magnetron sputtering”, Journal of Materials Science, 2010, 45(15), 4224–4228.

[4] Latha, H. K. E., Udayakumar, A, and Siddeswara Prasad V., “Microstructure and electrical properties of nitrogen doped 3C–SiC thin films deposited using methyl trichlorosilane. Materials Science in Semiconductor Processing, 2015, 29,117-123.

[5] Fang, H., Miller, T. M., Magruder, R. H., and Weller, R. A., “The effect of strain on the resistivity of indium tin oxide films prepared by pulsed laser deposition”, Journal of Applied Physics, 2002, 91(9), 6194–6196.

[6] Yeung, K. W., and Ong, C. W., “Micro-pressure sensors made of indium tin oxide thin films”, Sensors and Actuators A:

Physical, 2007, 137(1), 1–5.
[7] Wang, Y., Zhang, C., Juan, Li, Ding, Li, and Duan, G., "Fabrication and characterization of ITO thin film resistance temperature detector", Vacuum, 2016, 1-5.
[8] Hammad, T. M., "Effect of annealing on electrical, structural, and optical properties of sol-gel ITO thin films", Physica Status Solidi (A) Applications and Materials Science, 2009, 206(9), 2128–2132.
[9] Yadav, B. C., Agrahari, K., Singh, S., and Yadav, T. P., "Fabrication and characterization of nanostructured indium tin oxide film and its application as humidity and gas sensors", Journal of Materials Science: Materials in Electronics, 2016, 27(5), 4172–4179.
[10] Keum, M. J., and Han, J. G., "Preparation of ITO thin film by using DC magnetron sputtering", Journal of the Korean Physical Society, 2008, 53(3), 1580–1583.
[11] Lai, H. Y., Chen, T. H., and Chen, C. H., "Optical and electrical properties of inkjet printed indium-tin-oxide nanoparticle films", Materials Letters, 2011, 65(21–22), 3336–3339.
[12] Li, X., Xu, X., Yin, X., Li, C., and Zhang, J., "A sol-gel method to synthesize indium tin oxide nanoparticles", Particuology, 2011, 9(5), 471–474.
[13] Wang, H. W., Xu, G. D., Zhang, J. R., and Yin, X., "Hydrothermal synthesis of indium tin oxide nanoparticles without chlorine contamination", Bulletin of the Korean Chemical Society, 2014, 35(7), 1999–2003.
[14] Aziz, M. A., Zahir, M. H., Shaikh, M. N., Al-Betar, A. R., Oyama, M., and Sulaiman, K. O., "Hydrothermal synthesis of tin-doped indium oxide nanoparticles using pamoic acid as an organic additive and their photoluminescence properties", Journal of Materials Science: Materials in Electronics, 2017, 28(4), 3226–3233.
[15] Ding, Z., An, C., Li, Q., Hou, Z., Wang, J., Qi, H., and Qi, F., "Preparation of ITO nanoparticles by liquid phase coprecipitation method", Journal of Nanomaterials, 2010, 543601, 1-5.
[16] Sun, Z., He, J., Kumbhar, A., and Fang, J., "Nonaqueous synthesis and photoluminescence of ITO nanoparticles, Langmuir, 2010, 26(6), 4246–4250.
[17] Manafi, S., Tazikeh, S., and Joughehdoust, S., "Synthesis and characterization of indium tin oxide nanoparticles via reflux method", Materials Science- Poland, 2017, 35(4), 799–805.
[18] Ramasami, A. K., Reddy, M. V., and Balakrishna, G. R., "Combustion synthesis and characterization of NiO nanoparticles", Materials Science in Semiconductor Processing, 2015, Vol. 40, 194–202.
[19] Chavan, A.U., Kim, J.H., Im, H.N., and Song, S.J., "Role of different oxide to fuel ratios in solution combustion synthesis of SnO_2 nanoparticles", J. Korean Ceram. Soc. 53, 2016, 122–127.
[20] Huang, J.G., Zhuang, H.R., and Li W.L., "Synthesis and characterization of nano crystalline $BaFe_{12}O_{19}$ powders by low temperature combustion", Mater. Res. Bull., 2003, 38,149-159.
[21] Wang, H., Xu, X., Li, X., Zhang, J., and Li, C., "Synthesis and sintering of indium tin oxide nanoparticles by citrate-Nitrate combustion method", Rare Metals, 2010, 29(4), 355–360.
[22] Naika, H. R., Lingaraju, K., Manjunath, K., Kumar, D., Nagaraju, G., Suresh, D., and Nagabhushana, H., "Green synthesis of CuO NPs using Gloriosa superba L. extract and their antibacterial activity", In Journal of Taibah University for Science, 2015, Vol. 9, Issue 1, 7–12.
[23] Bhavyasree, P. G., and Xavier, T. S., "Green synthesis of Copper Oxide/Carbon nanocomposites using the leaf extract of Adhatoda vasica Nees, their characterization and antimicrobial activity", Heliyon, 2020, 6(2) e03323, 1-11.
[24] Rao, R., Chakra, C. H. S., and Rao, K. V., "Eco-friendly synthesis of silver nanoparticles using Carica papaya extract for anti-bacterial applications", Advanced Materials Research, 2013, 629(1), 279–283.
[25] Saha, P., Saha, N., Mahiuddin, M., and Islam, A. N., "Investigation on Fatty Acid Composition of Oil Extracted from Carica papaya Investigation on Fatty Acid Composition of Oil Extracted from Carica papaya L. Seed", International Journal of

Innovative Research in Science, Engineering and Technology, 2018, Vol. 7, Issue 10, 10543–10548.

[26] Baghi, R., Zhang, K., Wang, S., and Hope-Weeks, L. J., "Conductivity tuning of the ITO sol-gel materials by adjusting the tin oxide concentration, morphology and the crystalline size." Microporous and Mesoporous Materials, 2017, 244, 258-263.

[27] Thirumoorthi, M., and Thomas Joseph Prakash, J. "Structure, optical and electrical properties of indium tin oxide ultra-thin films prepared by jet nebulizer spray pyrolysis technique", Journal of Asian Ceramic Societies, 2016, 4(1), 124–132.

[28] Senthilkumar, V., Senthil, K., and Vickraman, P., "Microstructural, electrical and optical properties of indium tin oxide (ITO) nanoparticles synthesized by co-precipitation method", Materials Research Bulletin, 2012, 47(4), 1051–1056.

[29] Ayeshamariam, A., Vidhya, V. S., Sivakumar, T., Mahendran, R., Perumalsamy, R., Sethupathy, N., and Jayachandran, M., "nanoparticles of In_2O_3/SnO_2 (90/10) and (80/20) at Two Different Proportions and Its Properties", Open Journal of Metal, 2013, 03(02), 1–7.

[30] Mote, V., Purushotham, Y., and Dole, B., "Williamson-Hall analysis in estimation of lattice strain in nanometer-sized ZnO particles", J. Theor. Appl. Phys., 2012, 6, 2–9.

[31] Kosarian, A., Shakiba, M., and Farshidi, E., "Role of sputtering power on the microstructural and electro-optical properties of ITO thin films deposited using DC sputtering technique", IEEJ Transactions on Electrical and Electronic Engineering, 2018, 13(1), 27–31.

[32] Terzini, E., Thilakan, P., and Minarini, C., "Properties of ITO thin films deposited by RF magnetron sputtering at elevated substrate temperature", Materials Science and Engineering B: Solid-State Materials for Advanced Technology, 2000, 77(1), 110–114.

[33] Prasetya, A.T., Mursiti, S., Maryan, S., and Jati, N.K., "Isolation and Identification of Active Compounds from Papaya Plants and Activities as Antimicrobial", IOP Conf. Ser. Mater. Sci. Eng., 2018, 349, 1-6.

[34] Harinath Babu, S., Madhusudhana Rao, N., Kaleemulla, S., Amarendra, G., and Krishnamoorthi, C., "Room-temperature ferromagnetic and photoluminescence properties of indium-tin-oxide nanoparticles synthesized by solid-state reaction", Bulletin of Materials Science, 2017, 40(1), 17–23.

[35] Azam, A., Ahmed, A. S., Chaman, M., and Naqvi, A. H., "Investigation of electrical properties of Mn doped tin oxide nanoparticles using impedance spectroscopy", J. Appl. Phys., 2010, 108, 094329, 1-7.

[36] Jimenez Alvaro, R., Diana, N. D., and Morantes Maria, A., "Impedance analysis of TiO2 nanoparticles prepared by green chemical mechanism", Contemporary Engineering Sciences, 2018, 11(15), 737–744.

[37] Mubasher, Mumtaz, M., Hassan, M., Ali, L., Ahmad, Z., Imtiaz, M. A., Aamir, M. F., Rehman, A., and Nadeem, K., "Comparative study of frequency-dependent dielectric properties of ferrites MFe2O4 (M = Co, Mg, Cr and Mn) nanoparticles", Applied Physics A: Materials Science and Processing, 2020, 126(5), 334, 1-14.

[38] Bag, S., Das, P., and Behera, B., "AC impedance spectroscopy and conductivity studies of Dy doped Bi4V2O11 ceramics", Journal of Theoretical and Applied Physics, 2017, 11(1), 13–25.

[39] Dey, A., Dhar, J., Sil, S., Jana, R., and Ray, P. P., "Bias Voltage-Dependent Impedance Spectroscopy Analysis of Hydrothermally Synthesized ZnS nanoparticles", Journal of Materials Engineering and Performance, 2018, 27(6), 2727–2733.